Ocean dynamics, not dust, have controlled equatorial Pacific productivity over the past 500,000 years

Gisela Winckler[a,b,1], Robert F. Anderson[a,b], Samuel L. Jaccard[c,d], and Franco Marcantonio[e]

[a]Lamont-Doherty Earth Observatory, Columbia University, Palisades, NY 10964; [b]Department of Earth and Environmental Sciences, Columbia University, New York, NY 10027; [c]Institute of Geological Sciences, University of Bern, 3012 Bern, Switzerland; [d]Oeschger Center for Climate Change Research, University of Bern, 3012 Bern, Switzerland; and [e]Department of Geology and Geophysics, Texas A&M University, College Station, TX 77843

Edited by Edward A. Boyle, Massachusetts Institute of Technology, Cambridge, MA, and approved April 8, 2016 (received for review January 13, 2016)

Biological productivity in the equatorial Pacific is relatively high compared with other low-latitude regimes, especially east of the dateline, where divergence driven by the trade winds brings nutrient-rich waters of the Equatorial Undercurrent to the surface. The equatorial Pacific is one of the three principal high-nutrient low-chlorophyll ocean regimes where biological utilization of nitrate and phosphate is limited, in part, by the availability of iron. Throughout most of the equatorial Pacific, upwelling of water from the Equatorial Undercurrent supplies far more dissolved iron than is delivered by dust, by as much as two orders of magnitude. Nevertheless, recent studies have inferred that the greater supply of dust during ice ages stimulated greater utilization of nutrients within the region of upwelling on the equator, thereby contributing to the sequestration of carbon in the ocean interior. Here we present proxy records for dust and for biological productivity over the past 500 ky at three sites spanning the breadth of the equatorial Pacific Ocean to test the dust fertilization hypothesis. Dust supply peaked under glacial conditions, consistent with previous studies, whereas proxies of export production exhibit maxima during ice age terminations. Temporal decoupling between dust supply and biological productivity indicates that other factors, likely involving ocean dynamics, played a greater role than dust in regulating equatorial Pacific productivity.

climate change | export production | iron fertilization | carbon | eolian dust

Spanning nearly half the circumference of Earth, the equatorial Pacific represents one of the ocean's largest biogeographic provinces (1). Discovery of prominent Pleistocene cycles of carbonate ($CaCO_3$) abundance in equatorial Pacific sediments in the 1950s (2) launched one of the longest-running debates in paleoceanography. Arrhenius (2, 3) inferred that maxima in $CaCO_3$ abundance reflected greater biological productivity under ice age conditions, when intensification of the trade winds caused by steeper meridional global temperature gradients generated enhanced nutrient supply by upwelling. This view has been supported by a variety of complementary approaches, often based on the accumulation rate of organic carbon in equatorial Pacific sediments (e.g., refs. 4–7). On the other hand, studies involving microfossil preservation indices (8), spatial patterns of $CaCO_3$ accumulation (9, 10), and B/Ca ratios in benthic foraminifera as an indicator of carbonate ion concentration (11) have inferred a primary control on $CaCO_3$ cycles by varying deep ocean chemistry, which regulates $CaCO_3$ preservation, leaving unresolved the question of past variability of equatorial Pacific productivity and the conditions that regulate it.

A plausible role for dust in affecting productivity (e.g., refs. 12 and 13) can be invoked based on the following. First, biological utilization of major nutrients is limited by some other factor, especially in the eastern and central equatorial Pacific (14) where nutrients upwelled at the equator may spread poleward at the surface by more than five degrees of latitude before being completely consumed (15). Second, mesoscale iron (Fe) enrichment experiments have been shown to stimulate phytoplankton growth in the equatorial Pacific (16, 17). Lastly, the supply of dust, a source of Fe, was globally higher during the ice ages than during interglacials (18, 19), potentially reducing the growth-limiting effect of Fe deficiency.

Here, we evaluate the link between biological productivity and dust supply by establishing whether or not there were systematic changes in biological productivity throughout the past five glacial cycles, and whether these changes in productivity correlated with dust supply, as expected for the dust fertilization hypothesis.

Results and Discussion

We track dust flux and biological productivity, measured in the same sediment cores from the eastern equatorial Pacific [Ocean Drilling Program (ODP) site 849; 0.2°N, 110.5°W (19), this study] across the central equatorial Pacific [TT013-PC72; 0.1°N, 139.4°W (19–21)] to the western equatorial Pacific [RNDP74; 0.3°N, 159.4°E (22)] (Fig. 1 and Table S1). We primarily use the accumulation rate of excess barium (Ba_{xs}; see *Materials and Methods*) to reconstruct changes in export production, the flux of organic matter produced by biological productivity that rains from the euphotic zone to the deep ocean (Fig. 2). At one of the sites, TT013-PC72 in the central equatorial Pacific, where a record of opal, an independent proxy of export production, is available (13, 23), the accumulation rate of Ba_{xs} follows closely the accumulation rate of opal over the past 500 ky ($r = 0.7$, $P < 0.001$, Fig. S1). As the preservation of Ba_{xs} and opal are both variable and sensitive to multiple, but different, environmental factors, the correspondence of the two proxy records strongly supports their interpretation here as a robust representation of changes in export production (see also *Supporting Information*).

Throughout the past five glacial cycles, dust fluxes (reconstructed from accumulation rates of ^{232}Th; see *Materials and Methods*) at the three sites are closely correlated with $\delta^{18}O$ of foraminifera, which primarily tracks global ice volume (Fig. 2).

Significance

The equatorial Pacific is a key oceanographic region in Earth's climate system. Biological production in this region is limited, in part, by the lack of the micronutrient iron. Atmospheric dust is a source of iron, as is upwelling of ocean waters from below. A longstanding question has been whether biological productivity has responded to variable dust supply over ice age cycles. We use geochemical proxies in three sediment cores spanning the breadth of the equatorial Pacific to show that biological productivity did not respond to dustier ice age conditions. Rather than atmospheric iron supply, we infer that ocean dynamics, linking the equatorial Pacific to nutrient supply from the Southern Ocean, played a crucial role in regulating equatorial Pacific productivity.

Author contributions: G.W. and R.F.A. designed research; G.W. performed research; G.W. analyzed data; and G.W., R.F.A., S.L.J., and F.M. wrote the paper.

The authors declare no conflict of interest.

This article is a PNAS Direct Submission.

[1]To whom correspondence should be addressed. Email: winckler@ldeo.columbia.edu.

This article contains supporting information online at www.pnas.org/lookup/suppl/doi:10.1073/pnas.1600616113/-/DCSupplemental.

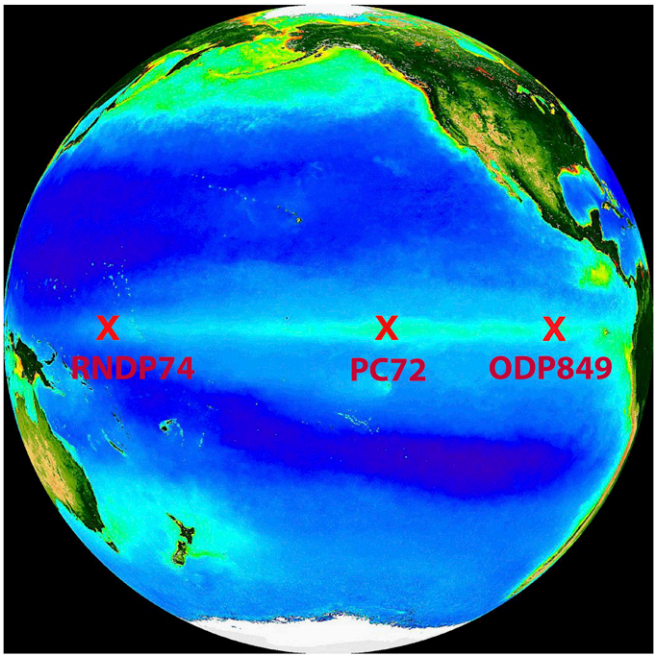

Fig. 1. Location of the three cores from the equatorial Pacific. Background map shows the surface water phytoplankton pigment concentration (oceancolor.gsfc.nasa.gov/SEAWIFS), which is interpreted to reflect primary production.

Dust fluxes are consistently about 2.5 times larger at peak glacial conditions than during interglacial periods (19, 20).

Whereas Ba_{xs} accumulation rates show variability of a factor of 2 at each of the sites, we do not observe systematically greater export production during glacial periods. Accumulation rates of Ba_{xs} are not correlated with dust flux (Fig. 2; for scatter plots, see Fig. S2). Given that we do not observe a systematic response of export production to greater ice age supply of dust, we reject the dust fertilization hypothesis for the equatorial Pacific.

The lack of a productivity response to changing dust fluxes is consistent with our understanding of the Fe budget in the present-day equatorial Pacific. Iron may be supplied to the euphotic zone from advective and diffusive processes within the ocean as well as by atmospheric deposition of mineral dust to the ocean surface. Iron contribution by upwelling (Fig. 3, Fig. S3, and *Supporting Information*) is found to be consistently much higher than eolian-derived Fe contributions, identifying upwelling from the Equatorial Undercurrent (EUC) as the principal source of Fe to the surface waters across most of the equatorial Pacific (24–26). Iron supply from upwelling is a factor of 20–100 greater than eolian sources for much of the central/eastern equatorial Pacific centered around site TT013-PC72 at 140°W (~160°W to 115°W). In the western equatorial Pacific (~160°E), where eolian input is higher, and at the eastern end of our transect (110°W), where dissolved Fe concentrations are lower, Fe input from upwelling is about a factor of 7–10 higher than eolian supply. Possible changes in the upwelling source or rate, as a result of changing ocean circulation, are therefore more likely to impact dissolved Fe supply to the surface ocean than the recorded 2.5-fold increase in dust-bound Fe deposition during glacials.

The dominant control on Fe supply by upwelling rather than dust holds true for past climates, as shown by the lack of a correlation ($r = 0.11$, $P = 0.16$, Fig. S4) between $\delta^{18}O$ and the accumulation rate of Fe (27) at TT013-PC72. Further support comes from the Fe/Th record at core TT013-PC72 (Fig. 3). Bulk sediment Fe/Th ratios are closely correlated to the ^{232}Th flux (Fig. 3*B*) and show cyclical variability between typical crustal Fe/Th ratios [~3,200 (28)] at maximum glacial conditions, when eolian input was the highest, and increased Fe/Th ratios during interglacial times. The enriched Fe/Th ratio requires an additional Fe source independent from eolian input, and we interpret this source to be upwelled dissolved Fe from the EUC, with a possible contribution from Papua New Guinea (PNG) volcanics carried eastward across the equatorial Pacific.

At TT013-PC72, multiple linear regression modeling of trace element and isotope data shows an upper limit for the contribution to total lithogenic deposition from PNG volcanics of 30% during the Holocene, and a much lower contribution during the Last Glacial Maximum and earlier glacial stages (29). In the following, we consider two limiting end-member scenarios to estimate the supply of Fe by upwelling (Fig. 3*C* and *Supporting Information*). For a constant maximum PNG lithogenic input, the best fit to the 500-ky time series Fe and Th data at 140°W requires a source of dissolved Fe from upwelling of 117 ± 7 $\mu mol \cdot m^{-2} \cdot y^{-1}$. Assuming no PNG supply of lithogenic material, the best fit corresponds to 167 ± 8 $\mu mol \cdot m^{-2} \cdot y^{-1}$. This sediment-based estimated range of dissolved Fe from upwelling by the EUC (Fig. 3*C*) is consistent with the modern hydrographic constraints of Fe upwelling (gray box at 140°W in Fig. 3*A*) and provides independent support for upwelling rather than dust as the dominant control on Fe supply in the equatorial Pacific.

The main feature in the record of export production across the equatorial Pacific is repeated increases in export productivity centered at glacial terminations (I, II, and IV; Figs. 4 and 2). Deglacial productivity maxima are consistent with previously observed peaks in opal flux at glacial terminations in the central equatorial Pacific (23) and similar findings, based on diatom/cocolithophore ratios (30) and carbon burial rates (31) in the easternmost equatorial Pacific.

Phytoplankton growth and utilization of nitrate (NO_3) and phosphate (PO_4) in the equatorial Pacific are colimited by Fe and by Si (32). Most of the Fe and all of the macronutrients (N, P, and Si) supplied to equatorial Pacific phytoplankton are delivered by upwelling of nutrient-rich water from the EUC. Therefore, the deglacial productivity maxima must reflect either an increase in the nutrient content of EUC water or an increase in the rate at which EUC water is upwelled into the euphotic zone.

Is there any evidence for increased nutrient concentrations of the EUC during the deglaciation? Most of the nutrients that fuel biological productivity in the tropical ocean, including the equatorial Pacific, originate in the Southern Ocean, where a portion of the nutrient-rich deep water that upwells south of the Antarctic Polar Front (APF) mixes northward to be entrained into Subantarctic Mode Water (SAMW), thereby feeding the upper thermocline nutrient source to low latitudes (33, 34). A southward displacement of the southern westerly winds, thought to have been responsible for the deglacial increase in upwelling of deep water south of the APF (35), would also have raised the nutrient content of SAMW based on historical observations (36). Silicon isotope records from core sites in the New Zealand sector of the Southern Ocean indicate higher nutrient concentrations in the SAMW source regions during the last deglaciation (37). At sites in the easternmost equatorial Pacific, east of 90°W, a deglacial peak in the nutrient content of EUC water during the last three ice age terminations has been inferred from the carbon isotope composition of thermocline-dwelling planktonic foraminifera (38, 39). The Nd isotope composition of the foraminfera from the same site indicates an increase in supply of Southern Ocean water to the EUC coincident with the rise in nutrient concentration (40).

Support for increased rates of upwelling during deglacial periods of greater export production, concurrently with a rise in the nutrient content of EUC water, comes from observations of the spatial and temporal variability of sea surface temperature at eastern equatorial Pacific sites (31, 41). Similarly, the nitrogen isotope composition of sedimentary organic matter in the eastern equatorial Pacific indicates a deglacial minimum in nitrate utilization coinciding with maximum export production,

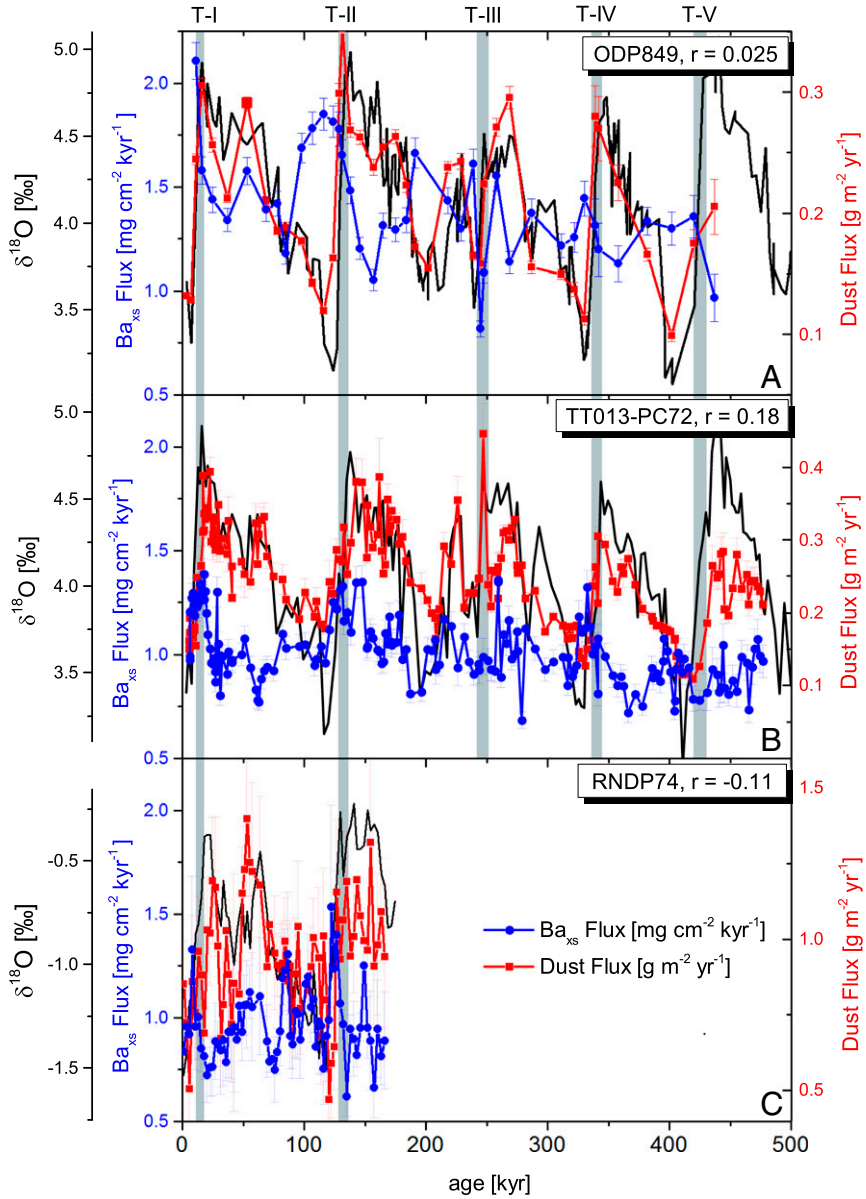

Fig. 2. Accumulation rates ($^{230}Th_{xs}$-normalized fluxes) of excess barium (Ba_{xs}, blue) and dust (red) at the three sites across the equatorial Pacific: (*A*) ODP site 849, (*B*) TT013-PC72, and (*C*) RNDP74. Dust fluxes are converted from $^{230}Th_{xs}$-normalized ^{232}Th fluxes by dividing by the average ^{232}Th concentration of upper continental crust (10.7 ppm; see *Materials and Methods*). Accumulation rates of Ba_{xs} are not correlated with dust flux [correlation coefficients of the Ba_{xs} and dust flux time series are 0.025 ($P = 0.88$), 0.18 ($P = 0.014$), and −0.11 ($P = 0.37$) in the eastern, central, and western Pacific, respectively]. The oxygen isotope records (black lines, *y* axis not reversed) are included for reference and define the glacial terminations as periods of rapid decrease in $\delta^{18}O$ (highlighted in gray bars).

a situation that requires an increase in supply of nutrients by upwelling (42).

The evidence for both increased nutrient content and increased upwelling is limited to observations from sites in the easternmost equatorial Pacific; unfortunately, corresponding proxy records are not available for our sites. Nevertheless, as the EUC supplies a uniform source of water, corresponding to uniform forcing throughout the upwelling system, we infer that the changes presented above for the easternmost equatorial Pacific likely extended to the entire central and eastern equatorial Pacific. Consequently, both factors, increased nutrient content of EUC water as well as increased rates of upwelling, likely contributed to the deglacial maxima in export production.

Although upwelled nutrients are not used immediately in the equatorial Pacific, they are eventually consumed completely and exported to depth as organic matter as surface waters mix poleward. Consequently, the biological pump in the equatorial Pacific is operating at full efficiency when integrated over appropriate temporal and spatial scales (15, 43). Neither natural variability of Fe sources in the past nor purposeful addition of Fe to equatorial Pacific surface water today, proposed as a mechanism for mitigating the anthropogenic increase in atmospheric CO_2 inventory, would have a significant impact on atmospheric pCO_2.

Materials and Methods

Reconstruction of Dust Supply. We use common thorium (^{232}Th), a trace element enriched in continental crust and low in basaltic volcanic material, as a tracer for lithogenic material, which, for cores far enough away from the continental margins, exclusively reflects eolian dust supply (19, 44). As ^{232}Th has very similar concentrations in dust sources from around the world, we

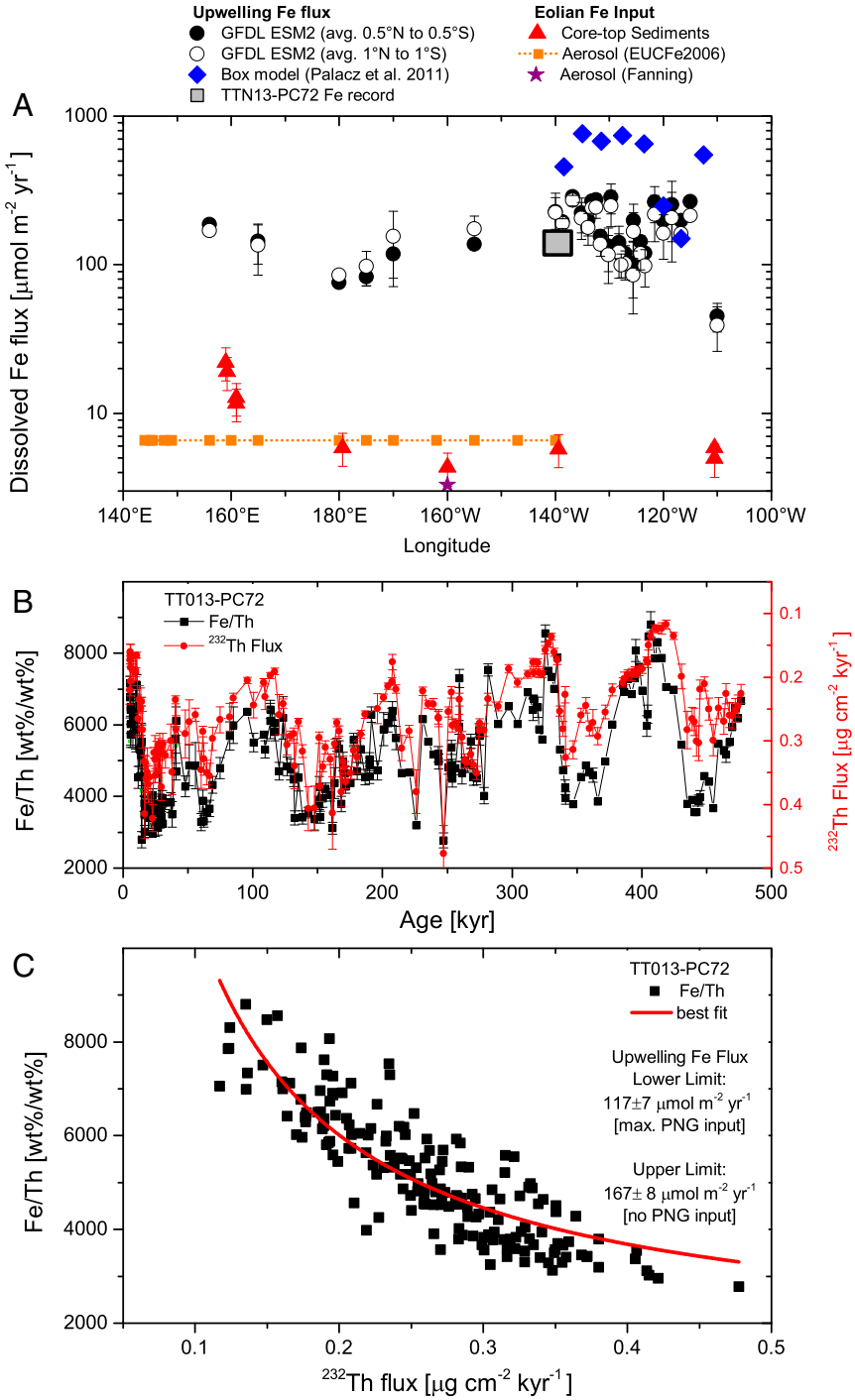

Fig. 3. Iron budget of the equatorial Pacific. (*A*) Compilation of upwelled Fe fluxes (using Fe concentration data from refs. 26 and 48 and vertical velocities from ref. 49; box model results from ref. 50) and eolian Fe fluxes [aerosol data from ref. 51 and Shank and Johansen (2008),* as cited in ref. 48; for details on core top sediment data compilation, see *Supporting Information*] illustrating that, over much of the equatorial Pacific, the input of Fe to surface waters from upwelling is much higher than that from eolian input. (*B*) Time series records of bulk sediment Fe/Th ratios (black) and ^{232}Th fluxes (red) at site TT013-PC72 over the past 500 ky. (*C*) The relationship between Fe/Th ratio and ^{232}Th fluxes reflects mixing of an eolian component, upwelling Fe from the EUC, and possible influence from PNG. The fit (see *Supporting Information* for details) requires EUC upwelling Fe fluxes between 117 ± 7 $\mu mol \cdot m^{-2} \cdot y^{-1}$ [assuming an upper limit (29) of PNG lithogenic ^{232}Th input of 0.015 $\mu g \cdot m^{-2} \cdot ky^{-1}$, assumed to be constant over the past 500 ky], and 167 ± 8 $\mu mol \cdot m^{-2} \cdot y^{-1}$ (assuming no sediment input from PNG). This range of upwelling Fe supply (gray square in *A*) is consistent with modern hydrographic estimates of Fe upwelling fluxes.

convert to dust mass fluxes by dividing by the average ^{232}Th concentration of upper continental crust (UCC), 10.7 ppm (28).

Reconstruction of Export Production. We use Ba_{xs} and opal to reconstruct variability in export production. The flux to the seabed of Ba_{xs}, the fraction of

*Shank LM, Johansen AM (2008) Atmospheric trace metal and labile iron deposition fluxes to the equatorial Pacific during EUCFe2006. Ocean Sciences Meeting, March 2–7, 2008, Orlando, FL.

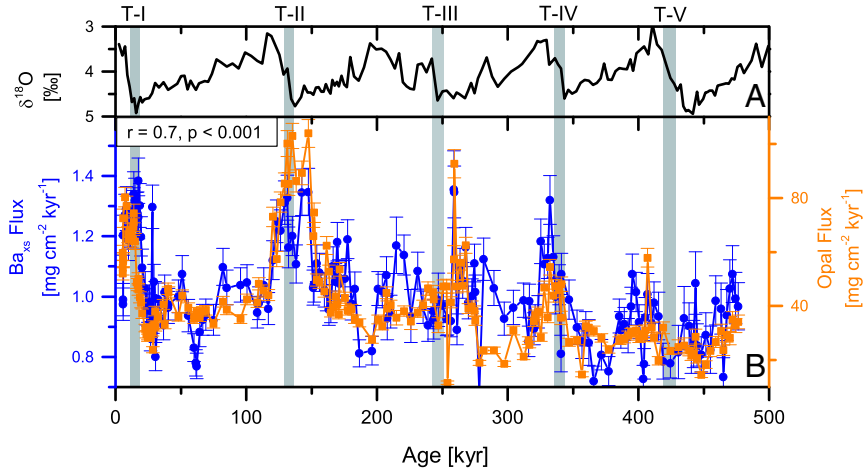

Fig. 4. Sedimentary records from the central equatorial Pacific site TT013-PC72. (*A*) Oxygen isotope record of benthic foraminifera (27); (*B*) $^{230}Th_{xs}$-normalized accumulation rates of excess barium (Ba data from ref. 21) and opal (opal data from ref. 23) illustrating deglacial peaks in export production at glacial Terminations I, II, and IV.

Ba that is not associated with lithogenic input, has been empirically shown to be strongly related to export production (e.g., refs. 45–47), because barite forms within aggregates of decomposing organic matter. Excess barium was calculated by subtracting the lithogenic Ba from the total Ba concentration using a $(Ba/Al)_{terrigeneous}$ ratio of 0.0075 (46). Corrections for the terrigeneous fraction are <1.5% at ODP site 849, <2.5% at TT013-PC72, and 3–8% at RNDP74 of the total measured barium in the sediments.

We present new Ba_{xs} data from ODP site 849 and integrate these with previously published U/Th data (19), as well as previously published Fe (27), Ba (21), and opal (23) data from site TT013-PC72, and Ba data from RNDP74 (22). Barium at ODP site 849 was measured by inductively coupled plasma mass spectrometry by isotope dilution at Lamont-Doherty Earth Observatory (LDEO). Data will be made available through the National Oceanic and Atmospheric Administration paleoclimatological data archive (National Climatic Data Center).

Reconstruction of Accumulation Rates. Accumulation rates of sedimentary constituents (Ba_{xs}, opal, Fe, ^{232}Th) were calculated using the $^{230}Th_{xs}$ method (for more details, see *Supporting Information*). Briefly, ^{230}Th is produced in the water column by the decay of ^{234}U at a known and constant rate. Thorium has a short residence time in the water column (20–40 y); it is adsorbed rapidly to settling particles and deposited in sediments at a rate that is fast relative to the timescale of lateral advection. Its scavenged flux to the seafloor can be assumed to be approximately equal to its known production rate in the overlying water column. Fluxes of sedimentary constituents (e.g., Ba_{xs}, opal, Fe, ^{232}Th) were calculated as the product of the concentration of the constituent, [i], and the $^{230}Th_{xs}$-derived mass accumulation rate.

Statistical Correlation. Correlations between time series are indicated by Pearson's correlation coefficient (r).

ACKNOWLEDGMENTS. We thank Roseanne Schwarz and Marty Fleisher for assistance in the lab. G.W. thanks Bernd Schwarz and Augusto Mangini for sharing the elemental and isotope data for RNDP 74. We thank Chris Measures for providing digital data from the EB04 cruise (see ref. 26), and Thomas Froelicher for providing upwelling rates extracted from the Geophysical Fluid Dynamics Laboratory (GFDL) model. This work was supported in part by several awards from the US NSF (to G.W. and R.F.A.). S.L.J. was supported by the Swiss National Science Foundation (Grant PP00P2_144811). This is LDEO contribution 7999.

1. Longhurst AR (2006) *Ecological Geography of the Sea* (Academic, New York).
2. Arrhenius GOS (1952) Sediment cores from the east Pacific. *Report of the Swedish Deep Sea Expeditions, 1947–1948* (Elander, Göteborg, Sweden), Vol 5, pp 1–228.
3. Arrhenius G (1988) Rate of production, dissolution and accumulation of biogenic solids in the ocean. *Paleogeogr Paleoclimatol Paleoecol* 67(1-2):119–146.
4. Lyle M (1988) Climatically forced organic carbon burial in the equatorial Atlantic and Pacific Oceans. *Nature* 335(6190):529–532.
5. Sarnthein MK, Winn K, Duplessy J-C, Fontugne MR (1988) Global variations of surface ocean productivity in low and mid latitudes: Influence on CO_2 reservoirs of the deep ocean and atmosphere during the last 21,000 years. *Paleoceanography* 3(3):361–399.
6. Paytan A, Kastner M, Chavez FP (1996) Glacial to interglacial fluctuations in productivity in the Equatorial Pacific as indicated by marine barite. *Science* 274(5291): 1355–1357.
7. Thomas E, Turekian KK, Wei K-Y (2000) Productivity control of fine particle transport to equatorial Pacific sediment. *Global Biogeochem Cycles* 14(3):945–955.
8. Lalicata JJ, Lea DW (2011) Pleistocene carbonate dissolution fluctuations in the eastern equatorial Pacific on glacial timescales: Evidence from ODP Hole 1241. *Mar Micropaleontol* 79(1-2):41–51.
9. Farrell JW, Prell WL (1991) Pacific $CaCO_3$ preservation and $\delta^{18}O$ since 4 Ma: Paleoceanic and paleoclimatic implications. *Paleoceanography* 6(4):485–498.
10. Anderson RF, Fleisher MQ, Lao Y, Winckler G (2008) Modern $CaCO_3$ preservation in equatorial Pacific sediments in the context of late-Pleistocene glacial cycles. *Mar Chem* 111(1-2):30–46.
11. Yu J, et al. (2013) Responses of the deep ocean carbonate system to carbon reorganization during the Last Glacial/Interglacial cycle. *Quat Sci Rev* 76:39–52.
12. Pichevin LE, et al. (2009) Enhanced carbon pump inferred from relaxation of nutrient limitation in the glacial ocean. *Nature* 459(7250):1114–1117.
13. Murray RW, Leinen M, Knowlton CW (2012) Links between iron input and opal deposition in the Pleistocene equatorial Pacific Ocean. *Nat Geosci* 5(4):270–274.
14. Barber RT, Chavez FP (1991) Regulation of primary productivity rate in the equatorial Pacific. *Limnol Oceanogr* 36(8):1803–1815.
15. Sigman DM, Haug GH (2003) The biological pump in the past. *The Oceans and Marine Geochemistry,* Treatise on Geochemistry, ed Elderfield H (Pergamom, Oxford), Vol 6, pp 491–528.
16. Coale KH, et al. (1996) A massive phytoplankton bloom induced by an ecosystem-scale iron fertilization experiment in the equatorial Pacific Ocean. *Nature* 383(6600):495–501.
17. Falkowski PG, Barber RT, Smetacek V (1998) Biogeochemical controls and feedbacks on ocean primary production. *Science* 281(5374):200–207.
18. Kohfeld KE, Harrison SP (2001) DIRTMAP: The geological record of dust. *Earth Sci Rev* 54(1-3):81–114.
19. Winckler G, Anderson RF, Fleisher MQ, McGee D, Mahowald N (2008) Covariant glacial-interglacial dust fluxes in the equatorial Pacific and Antarctica. *Science* 320(5872):93–96.
20. Anderson RF, Fleisher MQ, Lao Y (2006) Glacial-interglacial variability in the delivery of dust to the central equatorial Pacific Ocean. *Earth Planet Sci Lett* 242(3-4):406–414.
21. Murray RW, Knowlton C, Leinen M, Mix AC, Polsky CH (2000) Export productivity and carbonate dissolution in the central equatorial Pacific Ocean over the past 1 Myr. *Paleoceanography* 15(6):570–592.
22. Schwarz B, Mangini A, Segl M (1996) Geochemistry of a piston core from Ontong Java Plateau (western equatorial Pacific): Evidence for sediment redistribution and changes in paleoproductivity. *Geol Rundsch* 85(3):536–545.
23. Hayes CT, Anderson RF, Fleisher MQ (2011) Opal accumulation rates in the equatorial Pacific and mechanisms of deglaciation. *Paleoceanography* 26(1):PA1207.
24. Coale KH, Fitzwater SE, Gordon RM, Johnson KS, Barber RT (1996) Control of community growth and export production by upwelled iron in the equatorial Pacific. *Nature* 379(6566):621–624.
25. Gordon RM, Coale KH, Johnson KS (1997) Iron distributions in the equatorial Pacific: Implications for new production. *Limnol Oceanogr* 42(3):419–431.
26. Kaupp LJ, Measures CI, Selph KE, Mackenzie FT (2011) The distribution of dissolved Fe and Al in the upper waters of the Eastern Equatorial Pacific. *Deep Sea Res Part II Top Stud Oceanogr* 59(3-4):296–310.
27. Murray RW, Leinen M, Murray DW, Mix AC, Knowlton CW (1995) Terrigenous Fe input and biogenic sedimentation in the glacial and interglacial equatorial Pacific Ocean. *Global Biogeochem Cycles* 9(4):667–684.
28. Taylor SR, McLennan SM (1985) *The Continental Crust: Its Composition and Evolution* (Blackwell, Oxford).
29. Ziegler CL, Murray RW, Plank T, Hemming SR (2008) Sources of Fe to the equatorial Pacific Ocean from the Holocene to Miocene. *Earth Planet Sci Lett* 270(3-4):258–270.

30. Calvo E, Pelejero C, Pena LD, Cacho I, Logan GA (2011) Eastern equatorial pacific productivity and related-CO_2 changes since the last glacial period. *Proc Natl Acad Sci USA* 108(14):5537–5541.
31. Kienast M, et al. (2006) Eastern Pacific cooling and Atlantic overturning circulation during the last deglaciation. *Nature* 443(7113):846–849.
32. Brzezinski MA, et al. (2011) Co-limitation of diatoms by iron and silicic acid in the equatorial Pacific. *Deep Sea Res Part II Top Stud Oceanogr* 58(3-4):493–511.
33. Sarmiento JL, Gruber N, Brzezinski MA, Dunne JP (2004) High-latitude controls of thermocline nutrients and low latitude biological productivity. *Nature* 427(6969): 56–60.
34. Palter JB, Sarmiento JL, Gnanadesikan A, Simeon J, Slater RD (2010) Fueling export production: Nutrient return pathways from the deep ocean and their dependence on the Meridional Overturning Circulation. *Biogeosciences* 7(11):3549–3568.
35. Anderson RF, et al. (2009) Wind-driven upwelling in the Southern Ocean and the deglacial rise in atmospheric CO_2. *Science* 323(5920):1443–1448.
36. Ayers JM, Strutton PG (2013) Nutrient variability in Subantarctic Mode Waters forced by the Southern Annular Mode and ENSO. *Geophys Res Lett* 40(13):3419–3423.
37. Rousseau J, Ellwood MJ, Bostock H, Neil H (2016) Estimates of late Quaternary mode and intermediate water silic acid concentration in the Pacific Southern Ocean. *Earth Planet Sci Lett* 439:101–108.
38. Spero HJ, Lea DW (2002) The cause of carbon isotope minimum events on glacial terminations. *Science* 296(5567):522–525.
39. Pena LD, Cacho I, Ferretti P, Hall MA (2008) El Niño-Southern Oscillation-like variability during glacial terminations and interlatitudinal teleconnections. *Paleoceanography* 23(3): PA3101.
40. Pena LD, et al. (2013) Rapid changes in meridional advection of Southern Ocean intermediate waters to the tropical Pacific during the last 30 kyr. *Earth Planet Sci Lett* 368:20–32.
41. Kienast SS, et al. (2013) Near collapse of the meridional SST gradient in the eastern equatorial Pacific during Heinrich Stadial 1. *Paleoceanography* 28(4):663–674.
42. Robinson RS, Martinez P, Pena LD, Cacho I (2009) Nitrogen isotopic evidence for deglacial changes in nutrient supply in the eastern equatorial Pacific. *Paleoceanography* 24(4):PA4213.
43. Volk T, Hoffert MI (1985) Ocean carbon pumps: Analysis of relative strengths and efficiencies in ocean-driven atmospheric CO_2 changes. *The Carbon Cycle and Atmospheric CO_2: Natural Variations Archean to Present*, eds Sundquist ET, Broecker WS (American Geophys Union, Washington, DC), pp 99–110.
44. Rea DK (1994) The paleoclimatic record provided by eolian deposition in the deep sea: The geologic history of wind. *Rev Geophys* 32(2):159–195.
45. Dymond J, Suess E, Lyle M (1992) Barium in deep-sea sediment: A geochemical proxy for productivity. *Paleoceanography* 7(2):163–181.
46. Francois R, Honjo S, Manganini SJ, Ravizza GE (1995) Biogenic barium fluxes to the deep sea: Implications for paleoproductivity reconstructions. *Global Biogeochem Cycles* 9(2):289–303.
47. Winckler G, Anderson RF, Schlosser P (2005) Equatorial Pacific productivity and dust flux during the mid-Pleistocene climate transition. *Paleoceanography* 20:PA4025.
48. Slemons LO, Murray JW, Resing J, Paul B, Dutrieux P (2010) Western Pacific coastal sources of iron, manganese, and aluminum to the Equatorial Undercurrent. *Global Biogeochem Cycles* 24(3):GB3024.
49. Dunne JD, et al. (2012) GFDL's ESM2 global coupled climate–carbon Earth System Models. Part I: Physical formulation and baseline simulation characteristics. *J Clim* 25(19):6646–6665.
50. Palacz AP, Chai F, Dugdale RC, Measures CI (2011) Estimating iron and aluminum removal rates in the eastern equatorial Pacific Ocean using a box model approach. *Deep Sea Res Part II Top Stud Oceanogr* 58(5):311–324.
51. Prospero JM, Uematsu M, Savoie DL (1989) Mineral aerosol transport to the Pacific Ocean. *Chemical Oceanography* (Academic, San Diego), pp 188–218.
52. Warnock J, Scherer R, Loubere P (2007) A quantitative assessment of diatom dissolution and late quaternary primary productivity in the Eastern Equatorial Pacific. *Deep Sea Res Part II Top Stud Oceanogr* 54(5-7):772–783.
53. Bradtmiller LI, Anderson RF, Fleisher MQ, Burckle LH (2006) Diatom productivity in the equatorial Pacific Ocean from the last glacial period to the present: A test of the silicic acid leakage hypothesis. *Paleoceanography* 21(4):PA4201.
54. Johnson GC, McPhaden MJ, Firing E (2001) Equatorial Pacific Ocean horizontal velocity, divergence, and upwelling. *J Phys Oceanogr* 31(3):839–850.
55. Nakai S, Halliday AN, Rea DK (1993) Provenance of dust in the Pacific Ocean. *Earth Planet Sci Lett* 119:143–157.
56. Wu J, Liu Z, Zhou C (2013) Provenance and supply of Fe-enriched terrigenous sediments in the western equatorial Pacific and their relation to precipitation variations during the late Quaternary. *Global Planet Change* 108:56–71.
57. Whitmore GP, Crook KAW, Johnson DP (2004) Grain size control of mineralogy and geochemistry in modem river sediment, New Guinea collision, Papua New Guinea. *Sediment Geol* 171:129–157.
58. Tachikawa K, et al. (2011) The precession phase of hydrological variability in the Western Pacific Warm Pool during the past 400 ka. *Quat Sci Rev* 30(25-26):3716–3727.
59. Bacon MP (1984) Glacial to interglacial changes in carbonate and clay sedimentation in the Atlantic estimated from thorium-230 measurements. *Isot Geosci* 2:97–111.
60. Francois R, Frank M, Rutgers van der Loeff M, Bacon MP (2004) ^{230}Th normalization: An essential tool for interpreting sedimentary fluxes during the late Quaternary. *Paleoceanography* 19(1):PA1018.
61. Marcantonio F, Lyle M, Ibrahim R (2014) Particle sorting during sediment redistribution processes and the effect on ^{230}Th-normalized mass accumulation rates. *Geophys Res Lett* 41(15):5547–5554.
62. Marcantonio F, et al. (2001) Sediment focusing in the central equatorial Pacific Ocean. *Paleoceanography* 16(3):260–267.
63. Lyle M, et al. (2014) Sediment size fractionation and focusing in the equatorial Pacific: Effect on ^{230}Th normalization and paleoflux measurements. *Paleoceanography* 29(7): 747–763.
64. Mix AC, et al. (1995) Benthic foraminifer stable isotope record from Site 849 (0-5 Ma): Local and global climate changes. *Proceedings of the Ocean Drilling Program, Scientific Results*, eds Pisias NG, Mayer LA, Janecek TR, Palmer-Julson A, van Andel TH (Ocean Drill Program, College Station, TX), Vol 138, pp 371–412.
65. Marcantonio F, et al. (1995) A comparative study of accumulation rates derived by He and Th isotope analysis of marine sediments. *Earth Planet Sci Lett* 133:549–555.

Supporting Information

Winckler et al. 10.1073/pnas.1600616113

SI Results and Discussion

Reconstruction of Export Production Using Opal and Ba_{xs} Fluxes. The correlation between fluxes of opal and Ba_{xs} at TT013-PC72 supports their use as proxies for export production (Fig. S1). Opal and Ba_{xs} preservation in sediments is most sensitive to different environmental variables (temperature and redox conditions, respectively), so the internal consistency indicates that neither record has been compromised by variable preservation. Finding some scatter in the relationship is not surprising, considering that some export of organic matter, the decomposition of which regulates the formation of barite in the thermocline, is supported by phytoplankton taxa other than diatoms. Furthermore, variable silicification of diatoms under different environmental conditions may also have contributed to the observed scatter, but the overall good correlation indicates that variable silicification was a secondary factor influencing the opal flux record, if it occurred at all.

Although there is no direct proxy to constrain past changes in silicification, indirect evidence supports the view that it was minimal, if it occurred at all. Warnock et al. (52) found no glacial–interglacial change in diatom preservation in eastern equatorial Pacific sediments. One would expect diatom preservation to vary with silicification (positive correlation). The absence of any change in preservation argues against changes in silicification. Similarly, Bradtmiller et al. (53) showed that Pa/Th ratios are generally correlated with opal flux in the equatorial Pacific sediment downcore records. This is expected, due to the dominant role played by opal in scavenging Pa from seawater, but one would expect the correlation to break down if the sedimentary opal flux was strongly influenced by variable diatom silicification or by variable opal preservation. Combining evidence for no change in diatom preservation (52) with the evidence for a positive correlation between opal flux and Pa/Th (53), we can conclude that the opal flux record is not primarily influenced by variable diatom silicification or by variable opal preservation.

The Iron Budget in the Present-Day Equatorial Pacific. Dissolved iron (Fe) can be supplied to the euphotic zone of the equatorial Pacific by two processes: (*i*) via upwelling and (*ii*) via deposition of atmospheric mineral dust to the surface ocean and subsequent dissolution.

To constrain the Fe budget of the present-day equatorial Pacific, presented in Fig. 3, we compiled information available from the literature and evaluated (*i*) the relative contribution of Fe upwelling from the EUC and (*ii*) from atmospheric input from dust deposition.

Upwelling iron fluxes. Upwelling Fe fluxes can be determined based on dissolved iron concentration measurements, available from recent cruises to the western [EUCFe2006 (48)] and eastern [EB4, EB5 (26)] equatorial Pacific together with estimated vertical velocities [although upwelling in the equatorial Pacific is large compared with most other regions of the ocean, it is still much too small to be measured directly (54)].

We have combined dissolved Fe concentrations from the western and eastern equatorial Pacific in a zonal section spanning 150°E–110°W (Fig. S3*A*), and averaged Fe concentrations for subsurface waters (50–100 m) for each station (Fig. S3*B*). At 110°W and 140°W where meridional sections are available, we have averaged the Fe data over a 2° meridional band.

For the section from 140°W to 110°W, Palacz et al. (50) used a box model approach together with the dissolved Fe data from the EB4/EB5 cruise and estimated Fe upwelling fluxes on the order of 150–750 $\mu mol \cdot m^{-2} \cdot y^{-1}$ (Fig. 3*A*). To expand the estimate of Fe upwelling fluxes to the entire equatorial Pacific section from 150°E to 110°W, we have extracted the modeled vertical velocities from the Geophysical Fluid Dynamics Laboratory's (GFDL) Global Coupled Climate–Carbon Earth System Model 2 (ESM2), averaged for the interval 1985–2005 to filter out the high-frequency variability (ref. 49, Fig. S3*C*). We infer upwelling Fe fluxes across the equatorial Pacific by multiplying the subsurface (i.e., 50–100 m) Fe concentrations with the model-derived vertical velocities, averaged over the upper (i.e., 30–80 m) water column, across the equatorial Pacific (Fig. 3*A*). Although we acknowledge that the results may be model-dependent, this approach allows for a first-order consistent comparison of the strength of upwelled Fe input to the surface waters of the equatorial Pacific. In the eastern equatorial Pacific, the Fe upwelling fluxes calculated based on the GFDL ESM2 model velocities are up to a factor of 3 lower than the values derived by Palacz et al. As both analyses are based on the same Fe concentration data set (26) and performed at comparable depths in the water column, we interpret the difference between the two approaches to reflect a difference in the assumed upwelling rate, thus indicating that the upwelling rates from the GFDL ESM2 model are a conservative, time-averaged estimate, compared with the Palazc et al. box model.

Eolian iron input. We assess the atmospheric input of dissolved Fe to the equatorial Pacific surface ocean following three independent approaches: First, Shank and Johansen (2008)* analyzed aerosol filters, collected during the EUCFe2006 cruise, and estimated a dissolved Fe flux from dust of 6.6 $\mu mol \cdot m^{-2} \cdot y^{-1}$ averaged across the 150°E to 140°W section of the equatorial Pacific. Second, we compiled published thorium-based dust flux estimates from sediment core tops across the equatorial Pacific. Assuming a UCC average Fe/Th ratio of 3271 wt%/wt% (28) and an iron solubility of 6 ± 0.9% [determined from aerosol measurements from 4°N to 4°S from P16 cruise, cited after Kaupp et al. (26)], we estimate dissolved Fe input from eolian dust deposition of about 4–6 $\mu mol \cdot m^{-2} \cdot y^{-1}$ east of 160°W, and 11–22 $\mu mol \cdot m^{-2} \cdot y^{-1}$ in the western equatorial Pacific. This is consistent with modern iron flux estimates of 3.3 $\mu mol \cdot m^{-2} \cdot y^{-1}$ for 1981–1987 from the only aerosol station in the low-latitude Pacific on Fanning Island, located in the western equatorial Pacific [160°W, 3.9°N (51)].

The agreement between the ship aerosol analysis, the aerosol land station, and the core top-based reconstructions (from a variety of cores and laboratories) is very good, particularly when considering that these analyses integrate over very different timescales, short-term dust input in case of the aerosol filters and island station vs. long-term integrated dust fluxes over centuries–millennia for the sediment-based estimates.

Comparing upwelling iron fluxes with eolian iron fluxes. Across the equatorial Pacific from 160°E to 110°W, the Fe contribution from upwelling is consistently much higher than eolian-derived iron contributions, indicating that upwelling from the EUC is the principal source of iron to the surface waters of the equatorial Pacific (Fig. 3*A*). The difference between the two sources is highest in the middle section of the transect (160°W to 115°W) where the upwelling Fe flux is 20 to >100 times higher than the eolian contribution.

In the western (160°E) and eastern (110°W) equatorial Pacific, the relative difference is somewhat smaller, but upwelling fluxes remain about a factor of 7–10 higher than eolian input. We note that, in the eastern equatorial Pacific, between 115°W and 110°W, Fe concentrations drop off relatively abruptly. We do not have an extended data set for dissolved Fe east of 110°W to explore the iron budget. However, we note that the flux of dust to the equator at ~86.5°W, evaluated using an approach similar

to that used here, is about 3 times greater than the flux we determine at 140°W (41). If the trend of eastward decreasing dissolved Fe concentrations shown in Fig. S3*A* continues eastward, then dust may supply an increasing portion of the total Fe available to phytoplankton. We suggest that additional constraints are needed in the easternmost part of the equatorial Pacific to assess the role of ice age dust in regulating the productivity of the ecosystem in that region.

Iron sources constrained by sediment composition. As shown in Fig. 3 *B* and *C*, the Fe/Th ratios measured at core site TTN013-PC72 are closely correlated to the ^{232}Th flux (Fig. 3*B*) over the past 500 ky and show cyclical variability between low Fe/Th ratios at ^{232}Th flux maxima (glacial conditions) and high Fe/Th ratios at ^{232}Th minima (interglacial conditions). Measured Fe/Th ratios at times of maximum dust flux approach values for average UCC (3,271), which is expected if the main source of dust to this site is from East Asia (29, 55). Therefore, some source other than Asian dust must supply a major portion of the Fe accumulating in these sediments, and the proportional contribution from the other source(s) must be greatest during interglacial periods of minimum dust supply.

One possibility is that all of the nondust Fe is delivered as dissolved Fe transported by the EUC. The other end-member situation is that sediment with a much greater Fe/Th ratio is delivered to the site by the EUC (or by other currents). Sediment from PNG is a likely candidate, both because of its high Fe/Th ratio [~20,000 (29, 56, 57)] and because transport of PNG sediment to the site of TT013-PC72 would be facilitated by the same EUC system that delivers dissolved Fe. Although PNG has the required high Fe/Th ratio, a simple mass balance based on Nd isotopes informs us that the nondust Fe cannot be entirely associated with PNG sediment. As shown by Ziegler et al. (29), the maximum contribution of PNG sources to the total lithogenic material in TT013-PC72 is ~30% during interglacials and much less during glacials. This can be derived using the Nd isotopic composition of PNG sediment ($\varepsilon_{Nd} \approx +7$) and that of Asian dust sources ($\varepsilon_{Nd} \approx -10$), the likely source of eolian material delivered to the core site. Further considering that PNG sediment and Asian dust have similar Nd concentrations (~30 ppm), the measured isotopic composition of lithogenic material in TT013-PC72 ($\varepsilon_{Nd} \approx -5$) allows a maximum contribution of 30% PNG sediment during interglacials, and less during glacials.

Assuming that up to three principal sources (dust, PNG sediment, and dissolved Fe carried by the EUC) deliver Fe and Th to the sediments at the site of TT013-PC72, we use the least squares fit to the relationship between bulk sediment Fe/Th ratio and ^{230}Th-normalized ^{232}Th flux (Fig. 3*C*) to constrain the supply of dissolved Fe carried by the EUC as well as the Fe/Th ratio of the dust source. We evaluate these parameters for two end-member situations: one for which there is no supply of PNG sediment and one for which the supply of PNG sediment is constant through time and equivalent to 30% of the total supply of lithogenic material during interglacials (an upper limit; see above and ref. 29). In each case, the relationship has the form $Y = A/X + B$, where Y is the bulk sediment Fe/Th ratio and B is the Fe/Th ratio of dust.

In the first case, with no PNG sediment and further assuming no significant supply of dissolved Th by the EUC, we have

$$\left(\frac{Fe}{Th}\right)_{bulk-sediment} = \left(\frac{F_{Fe-EUC} + F_{Fe-dust}}{F_{Th-dust}}\right) = \left(\frac{F_{Fe-EUC}}{F_{Th-dust}}\right) + \left(\frac{Fe}{Th}\right)_{dust}.$$

Here, F refers to flux to the core site and A is the supply of dissolved Fe by the EUC ($F_{Fe\text{-}EUC}$), which is estimated from the least squares fit to be 167 ± 8 μmol·m^{-2}·y^{-1}.

In the second case, assuming no supply of dissolved Th by the EUC and a constant source of PNG sediment, equivalent to 30% of the total interglacial supply of lithogenic material to the site of TT013-PC72, the mass balance is

$$\left(\frac{Fe}{Th}\right)_{bulk-sediment} = \left(\frac{F_{Fe-EUC} + F_{Fe-PNG} + F_{Fe-dust}}{F_{Th-PNG} + F_{Th-dust}}\right).$$

Rearranging the right-hand side yields

$$\left(\frac{Fe}{Th}\right)_{bulk-sediment} = \frac{F_{Fe-EUC} + F_{Th-PNG} \cdot \left[\left(\frac{Fe}{Th}\right)_{PNG} - \left(\frac{Fe}{Th}\right)_{dust}\right]}{F_{Th-PNG} + F_{Th-dust}} + \left(\frac{Fe}{Th}\right)_{dust}.$$

Again, the form of the equation is $Y = A/X + B$ and $B = (Fe/Th)_{dust}$. X is the total supply of Th to the sediment (PNG + dust), and

$$A = F_{Fe-EUC} + F_{Th-PNG} \cdot \left[\left(\frac{Fe}{Th}\right)_{PNG} - \left(\frac{Fe}{Th}\right)_{dust}\right].$$

We evaluate the supply of dissolved Fe by the EUC ($F_{Fe\text{-}EUC}$) by rearranging the equation above after substituting the numerical values for A and B [$(Fe/Th)_{dust}$] obtained by best fit to the data in Fig. 3*C*, the value for $(Fe/Th)_{PNG}$ [~20,000 (29, 56, 57)], and $F_{Th\text{-}PNG}$ (0.015 μg·m^{-2}·ky^{-1}), which is derived assuming a constant flux of PNG sediment equal to 30% of the total interglacial lithogenic supply and a Th content of 3.5 ppm (57). This end member yields a lower limit for the supply of dissolved Fe by the EUC of 117 ± 7 μmol·m^{-2}·y^{-1}.

The Fe/Th ratio of the dust end member, implied by the mixing relationship in Fig. 3*C*, is about half of the UCC average of 3,271 (28), used above to estimate modern eolian iron fluxes.

Our estimate of the low Fe/Th ratio for the dust end member obtained from the statistical fit to the data in Fig. 3*C* relies on the assumption of a constant supply over time of sediment derived from PNG. Instead, if the supply of PNG sediment to 140°W decreased systematically during glacial periods or on some other climate-related cyclicity (e.g., ref. 58), then the estimated Fe/Th ratio of the dust end member would increase accordingly, approaching the UCC value in the absence of any input of PNG sediment. Further work is needed to establish whether the dust delivered to 140°W has a Fe/Th ratio roughly half that of UCC, or if the supply of PNG sediment to 140°W varies systematically with climate, with supply of PNG sediment decreasing, perhaps to negligible levels, during glacial periods. In either case, as noted above, any realistic departure from our assumption of an UCC value for the Fe/Th ratio of dust in estimating the eolian source of Fe to the equatorial Pacific would reduce the level of dust-derived Fe illustrated in Fig. 3*A*, further widening the gap between Fe supplied by upwelling and Fe delivered by dust. Accordingly, using the UCC ratio for estimating the eolian iron input from core top sediment data (Fig. 3*A*) provides a conservative upper limit of eolian Fe fluxes.

Reconstruction of Accumulation Rates by Thorium Normalization.

Reconstruction of accumulation rates using the $^{230}Th_{xs}$ method. Accumulation rates of sedimentary constituents (Ba_{xs}, opal, Fe, ^{232}Th) are calculated using the $^{230}Th_{xs}$ method (59, 60). Thorium-230 is produced in the water column by the decay of ^{234}U at a known and constant rate. Thorium has a short residence time in the water column (20–40 y); it is adsorbed rapidly to settling particles and deposited in sediments at a rate that is fast relative to the timescale of lateral advection. Its scavenged flux to the seafloor can be assumed to be approximately equal to its known production rate in the overlying water column. Sedimentary concentrations of $^{230}Th_{xs}$ are therefore inversely proportional to the vertical rain rate of sediments.

The $^{230}Th_{xs}$-normalized mass accumulation rate (*MAR*) for each sample is

$$MAR = \frac{\beta \cdot z}{[^{230}Th_{xs}]}$$

where β is the constant ^{230}Th production rate in seawater, z is the water depth in meters, and $[^{230}Th_{xs}]$ is the measured ^{230}Th activity after corrections for ^{230}Th supported by ^{238}U in detrital sediments, ^{230}Th supported by authigenic ^{238}U precipitated from seawater, and radioactive decay since deposition.

Fluxes of sedimentary constituents (e.g., Ba_{xs}, opal, Fe, ^{232}Th) are calculated as the product of the concentration of the constituent, [i], and the mass accumulation rate,

$$F = [i] \cdot MAR.$$

Our analysis of $^{230}Th_{xs}$-normalized accumulation rates is limited to proxies in the fine fraction of the sediments, which is not sensitive to the recently reported fractionation of coarse (carbonate) fraction during sediment redistribution (61). We also note that the consistency of correlations (and lack thereof) across the equatorial Pacific illustrates that this is not a specific effect at any one site but a consistent pattern observed across varying regimes of the entire tropical Pacific.

The $^{230}Th_{xs}$ normalization method offers several advantages over stratigraphic accumulation rates (59, 60), which rely on the mass of sediment accumulated between age control points. Most significantly, the $^{230}Th_{xs}$ normalization method corrects for syndepositional redistribution of sediment by deep-sea currents (sediment focusing). The method does not require knowledge of in situ sediment density, and it is relatively insensitive to small (few kiloyears) errors in age control points. Lastly, the $^{230}Th_{xs}$ normalization method allows the evaluation of preserved sediment flux at every sample depth, in contrast to the stratigraphic accumulation method, which provides average accumulation rates between each pair of age control points.

Comparison with stratigraphy-derived results. Our ^{230}Th-normalized results are inconsistent with previous work inferring large maxima in export production during peak glacial conditions based on stratigraphic Ba_{xs} (and barite) bulk MARs (BMARs) (6), i.e., accumulation rates derived from linear sedimentation rates calculated between δ^{18}O-dated depth horizons. We reproduce pronounced changes in stratigraphy-based Ba_{xs} fluxes at all three sites (Fig. S5), similar to the previously reported results at TTN013-PC72 (6). We also find that the Ba_{xs} BMARs are strongly correlated to stratigraphic ^{232}Th BMARs (for scatter plots, see Fig. S2 *D–F*). However, these correlations disappear when the proxy concentrations are normalized to $^{230}Th_{xs}$ (Fig. 2 and Fig. S2 *A–C*), and there is consistently no correlation between export production and dust input. Similarly, strong links between opal BMAR and iron BMAR have been inferred (13) based on stratigraphic mass accumulation rates (BMARs, Figs. S4*E* and S6*B*). The correlation disappears when opal and iron are normalized to ^{230}Th (Figs. S4*B* and S6*A*).

We hypothesize that the correlation between the stratigraphic accumulation rates of Ba_{xs} and ^{232}Th (Fig. S2 *D–F*), as well as the correlation between the stratigraphic accumulation rates of iron and opal (Fig. S4*E*), is related to a combination of the following potential artifacts: First, because $CaCO_3$ is the main phase in these sediments and controls the concentrations of all other phases, including opal, Fe, ^{232}Th, Ba, and $^{230}Th_{xs}$ (Figs. S6*C* and S7, and scatter plots in Fig. S8), variable dilution by $CaCO_3$ may lead to apparent correlations. Second, maxima in stratigraphy-derived Ba_{xs} and ^{232}Th BMARs, as well as in Fe and opal BMARs, correspond to $CaCO_3$ minima (Fig. S6). Loss of $CaCO_3$ by dissolution may impose systematic errors on the δ^{18}O-derived age model whereby the apparent duration of $CaCO_3$-poor intervals is artificially shortened by the loss of foraminifera deposited during those periods, thus creating an erroneously large apparent BMAR. A third potential factor is climate-related variability in sediment redistribution (e.g., refs. 60, 62, and 63).

Normalizing the proxy data to $^{230}Th_{xs}$ avoids artifacts related to carbonate dissolution and correctly represents vertical fluxes that may have been modified by sediment redistribution.

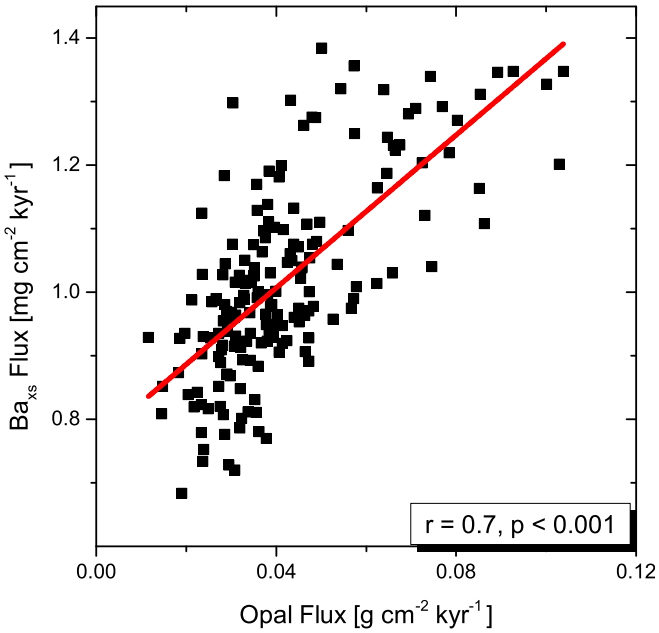

Fig. S1. Correlation between the ^{230}Th-normalized accumulation rate of excess Ba and opal at the central equatorial Pacific site, TT013-PC72. The accumulation rate of excess barium follows closely the accumulation rate of opal over the past 500 ky, indicated by a correlation factor of $r = 0.7$ ($P < 0.001$). The internal consistency, despite differing sensitivity of the preservation of Ba_{xs} and opal to deep-sea environmental conditions, supports their use as proxies for export production.

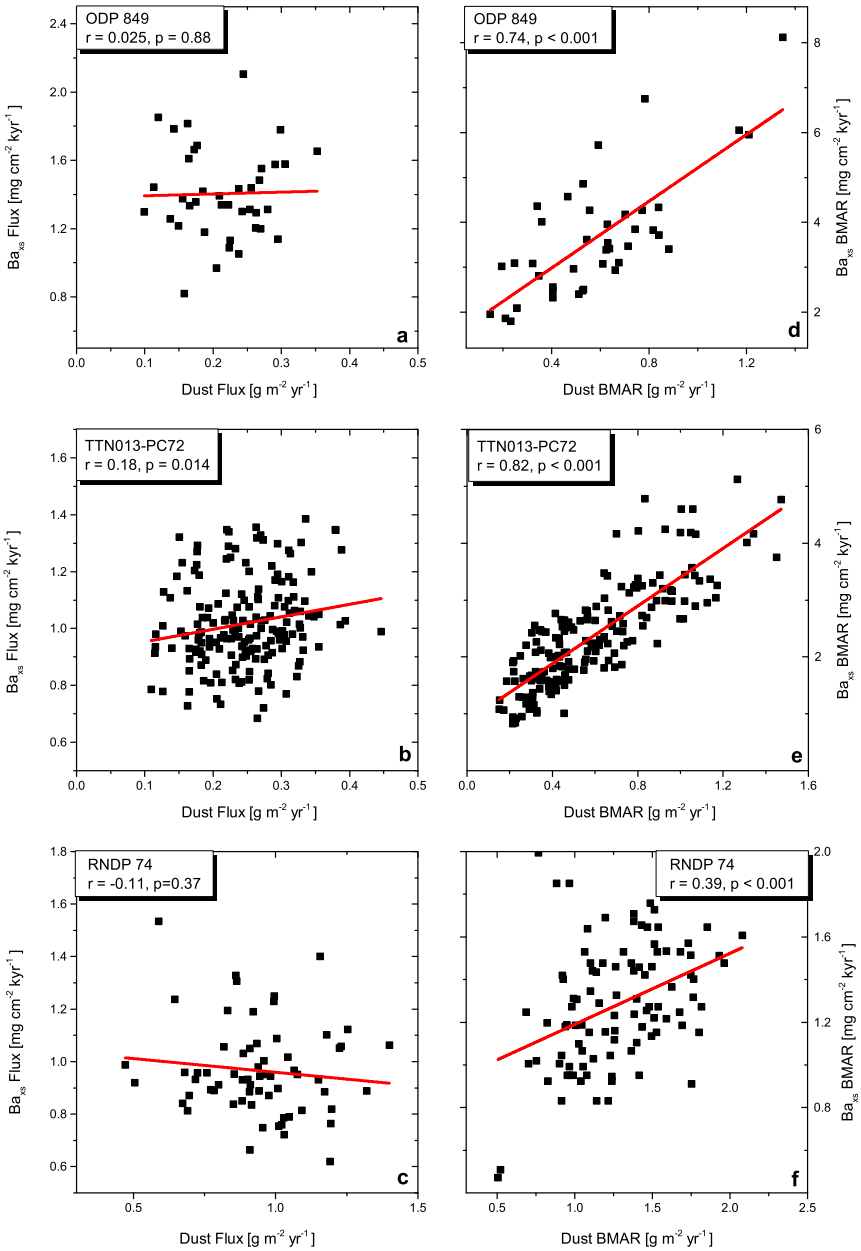

Fig. S2. Correlations between excess barium and dust at the three locations (*A* and *D*, ODP 849; *B* and *E*, TT013-PC72; and *C* and *F*, RNDP 74) using $^{230}Th_{xs}$-normalized accumulation rates (*A*–*C*) and stratigraphic accumulation rates (*D*–*F*). No significant correlations between export production and dust flux are observed in $^{230}Th_{xs}$-normalized rates (*A*–*C*). Positive correlations observed for stratigraphic rates (*D*–*F*) are due to artifacts related to some combination of carbonate dissolution, sediment redistribution, or errors in age models.

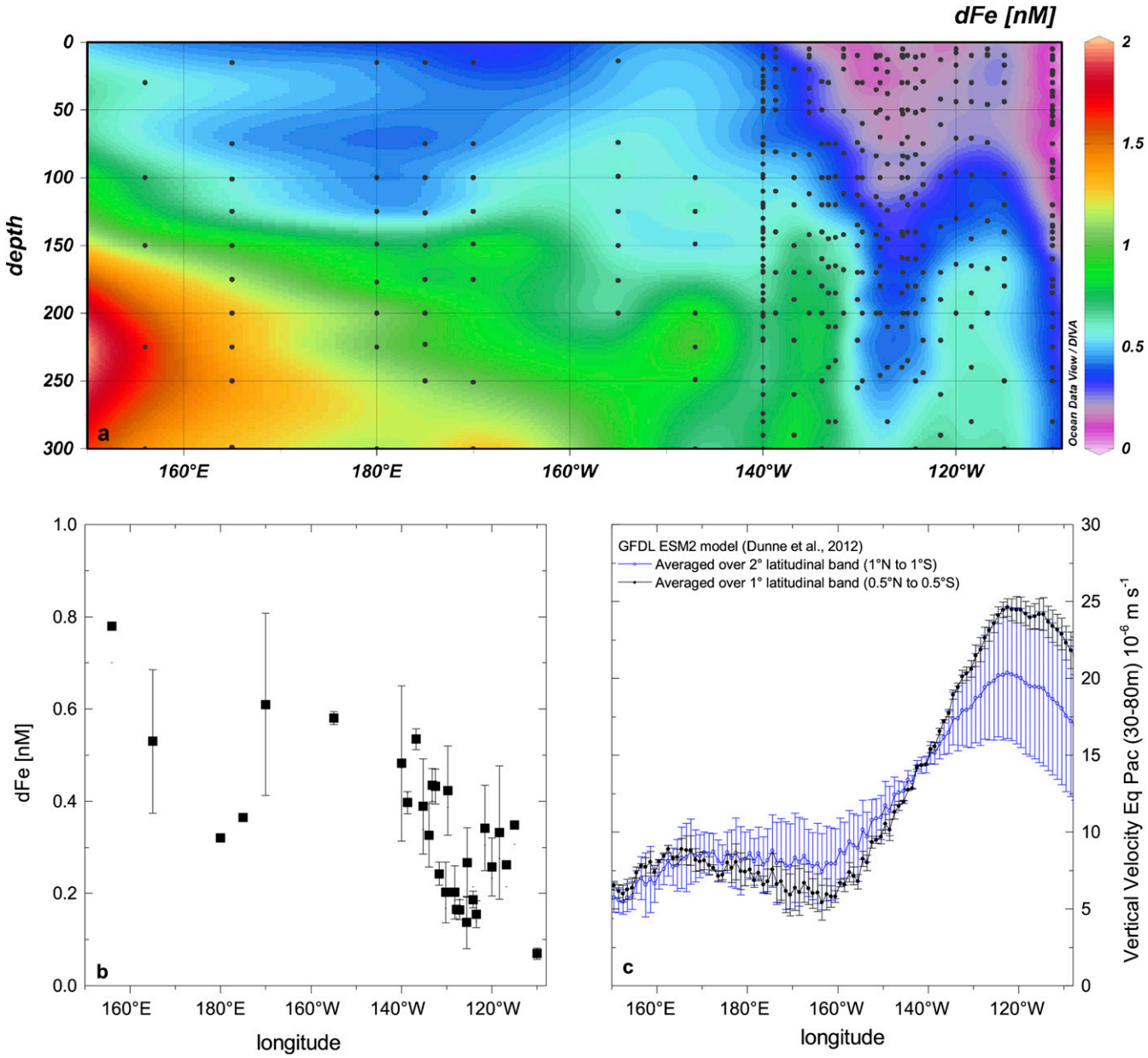

Fig. S3. (*A*) Zonal section of dissolved iron concentrations along the equator from 150°E to 110°W [data from Slemons et al. (48) and Kaupp et al. (26)]. (*B*) Averaged Fe concentrations (50–100 m), with the errors representing the SD of the data. (*C*) Vertical velocities (averaged over 30–80 m) from GFDL ESM2M model (49), averaged over a 1° and a 2° meridional band. Upwelling rates are about a factor of 2–4 lower in the western equatorial Pacific than in the eastern equatorial Pacific, with the west–east gradient being more pronounced closer to the equator (1° band) than in the 2° meridional band.

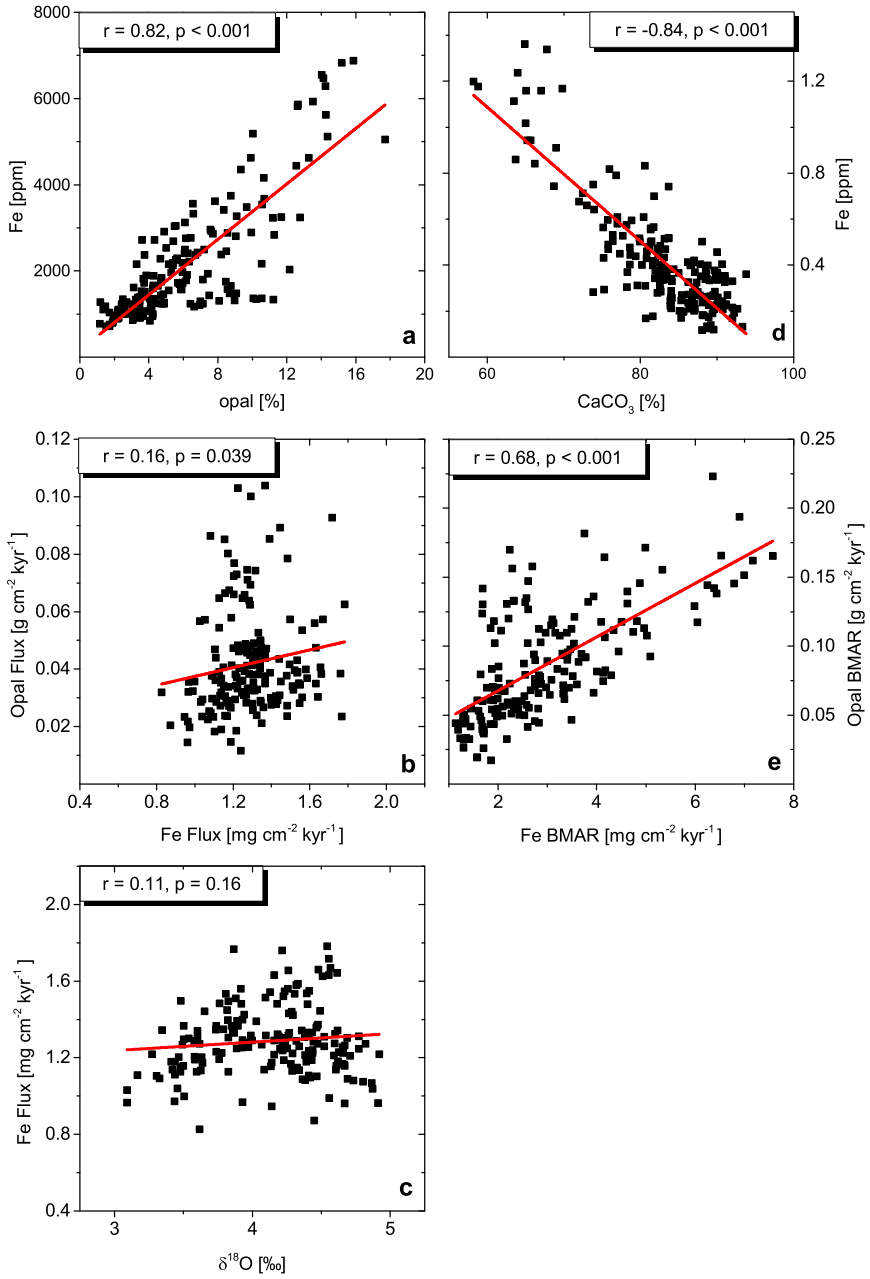

Fig. S4. Correlation between iron and opal, and their accumulation rates at the central equatorial Pacific site TT013-PC72. Iron is highly correlated with opal concentration (*A*) and calcium carbonate (*D*). However, ^{230}Th-normalized opal fluxes are not correlated to iron supply (*B*). The apparent correlation, observed between the stratigraphic opal and iron accumulation rate (*E*), is due to artifacts, related to carbonate dissolution and/or sediment redistribution. We do not observe a significant correlation between Fe flux and δ^{18}O over the past 500 ky (*C*), in contrast to ^{232}Th flux (dust proxy) and δ^{18}O (Fig. 2*B*). The absence of a correlation between Fe flux and δ^{18}O indicates a substantial source of Fe that is not associated with dust, which we attribute to supply by upwelling from the EUC.

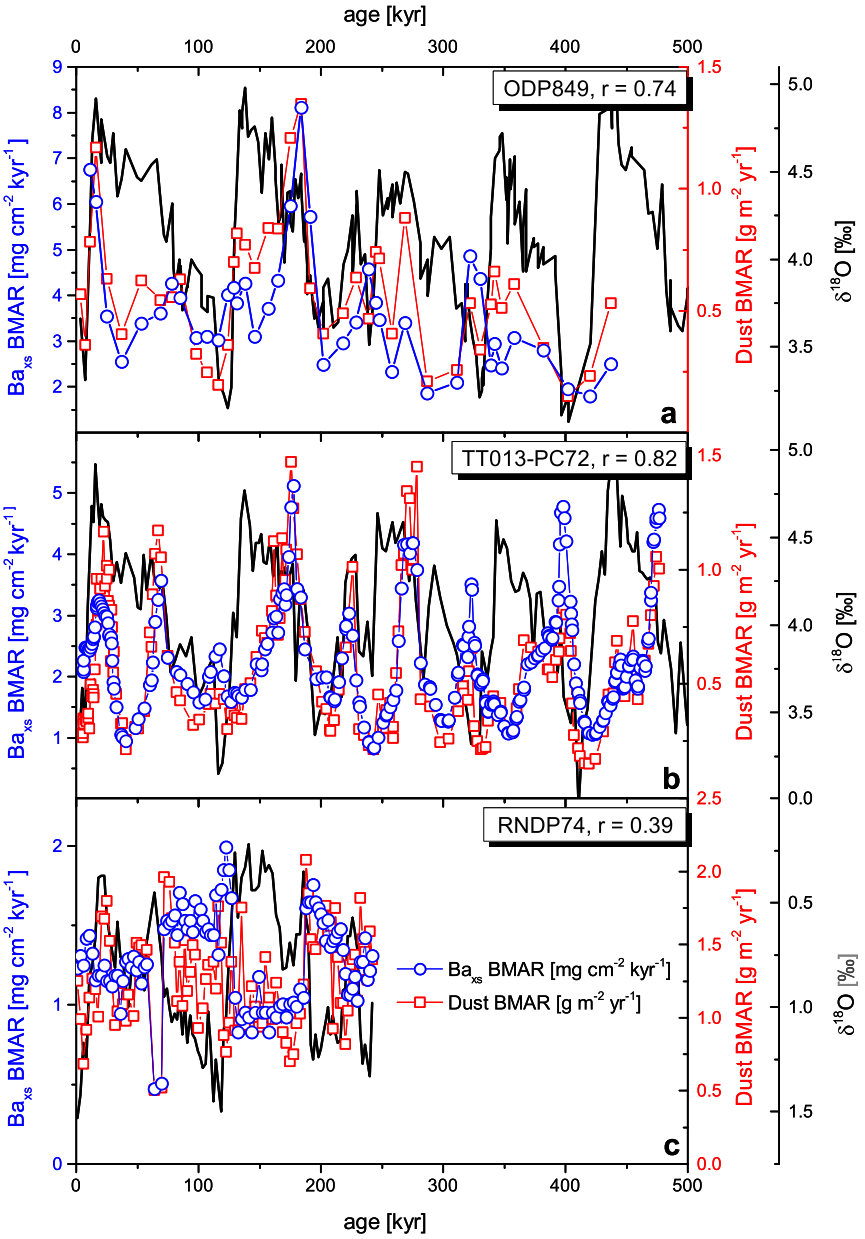

Fig. S5. Stratigraphic accumulation rates (BMAR) of excess barium (blue) and dust (red) for the three sites: (*A*) ODP 849, (*B*) TT013-PC72, and (*C*) RNDP 74. The oxygen isotope records (black lines, *y* axis not reversed) are included for reference. Stratigraphic Ba_{xs} accumulation rates are strongly correlated to stratigraphic dust accumulation rates but not to the climate signal. Correlation factors are indicated in each panel, all $P < 0.001$. The apparent correlations may be related to a combination of the following potential artifacts: (*i*) variable dilution by $CaCO_3$, the main phase in the sediments; (*ii*) the effect of the loss of $CaCO_3$ by dissolution on δ^{18}O-derived age models (e.g., by apparently shortening the duration of $CaCO_3$-poor intervals); and (*iii*) variability in sediment redistribution.

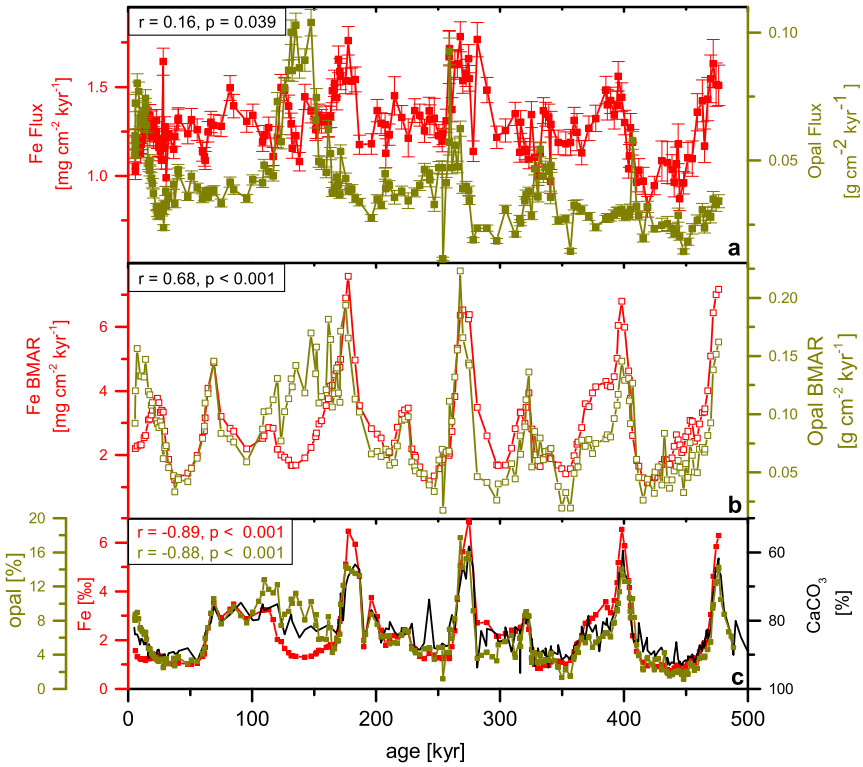

Fig. S6. Iron and opal records from the central equatorial Pacific site TT013-PC72. (*A*) The $^{230}Th_{xs}$-normalized accumulation rates of iron (red, Fe data from ref. 27) and opal (dark yellow, from ref. 23). (*B*) Stratigraphic mass accumulation rates (BMAR, open symbols) of iron (27) and opal (23). (*A* and *B*) Correlation coefficients of accumulation rate time series are indicated. (*C*) Iron concentration (red, from ref. 27) and opal concentration (dark yellow, from ref. 23, left *y* axis) vs. calcium carbonate content (black, right *y* axis, reversed scale). Correlation coefficients of opal (dark yellow) and iron concentrations (red) with $CaCO_3$ content are given.

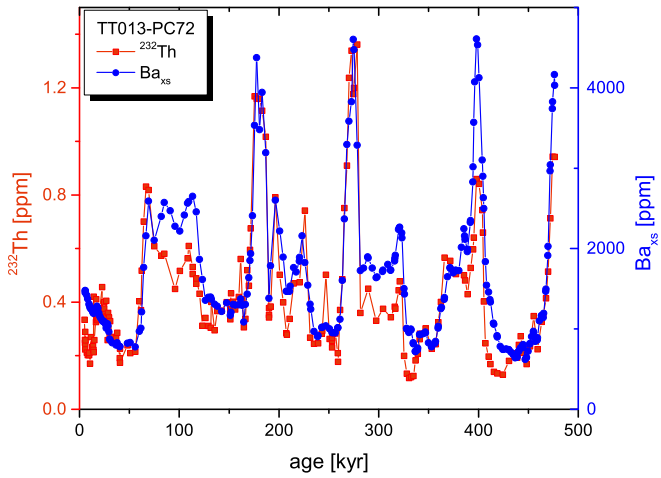

Fig. S7. Time series of Ba_{xs} (blue) and ^{232}Th (red) at the central equatorial Pacific site TT013-PC72. The concentrations of ^{232}Th and Ba_{xs} are dominated by dilution with calcium carbonate (as are all other sedimentary constituents). By normalizing the proxies for dust and for productivity to ^{230}Th, we correct for the variable dilution with $CaCO_3$ and can then compare meaningful fluxes of these components.

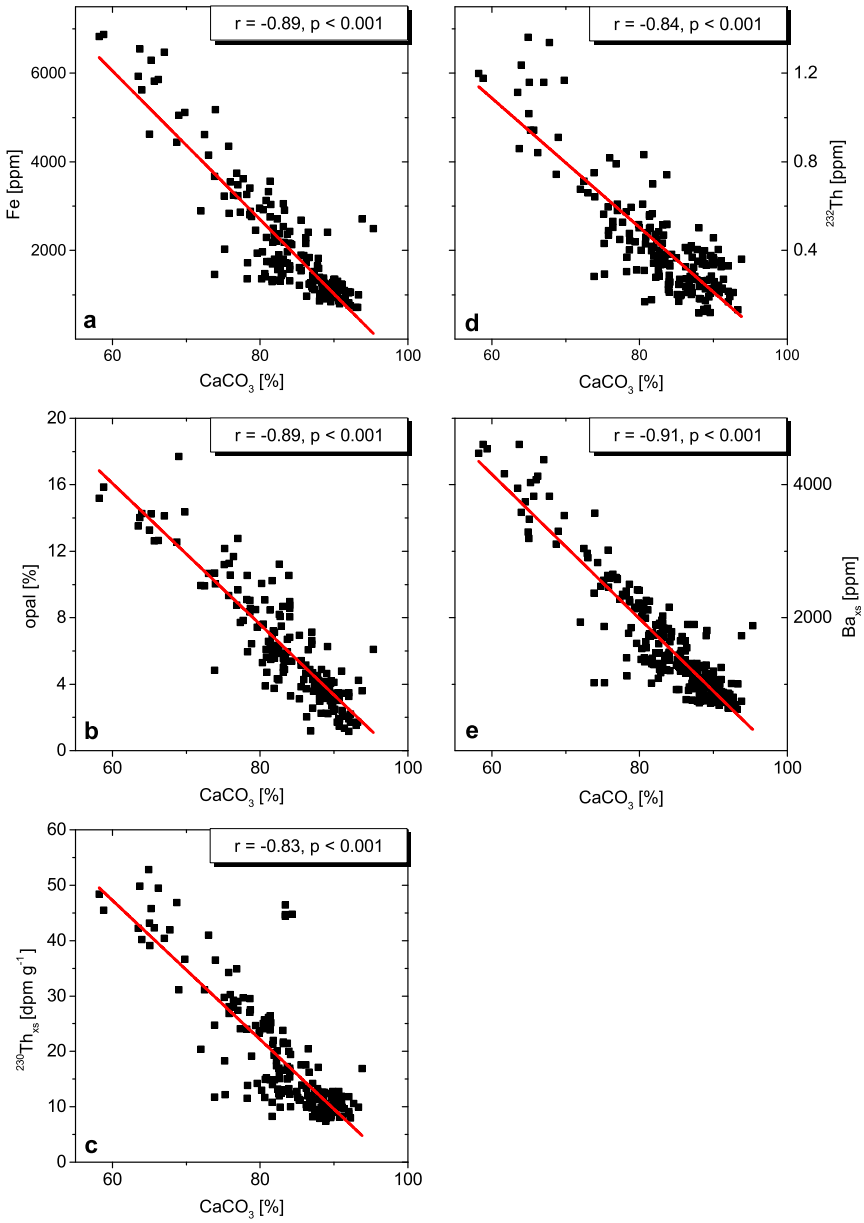

Fig. S8. Correlation between sedimentary constituents and calcium carbonate, the dominant component of the sediments, at the central equatorial Pacific site, TTN013-PC72. (*A*) Fe, (*B*) opal, (*C*) ^{230}Th, (*D*) ^{232}Th, and (*E*) Ba_{xs}, respectively, vs. $CaCO_3$. All components are highly correlated with $CaCO_3$ (see correlation factors, all $P < 0.001$), indicating that dilution by variable calcium carbonate preservation is the primary control on the concentration of all components, including lithogenic (^{232}Th), biogenic (opal, Ba_{xs}), and authigenic ($^{230}Th_{xs}$, decay corrected to time of deposition) constituents as well as iron, which is supplied from multiple sources.

Table S1. Core locations and data sources

Core	Location	Age model	$\delta^{18}O$*	U/Th isotopes	Ba_{xs}	Opal	Fe
ODP 849 (3,839 m)	0.2°N,110.5°W	(64)	(64)	(19)	this study	n/a[§]	n/a
TT013-PC72 (4,298 m)	0.1°N,139.4°W	(27)[†]	(21)	(19, 20, 65)	(21)	(23)	(27)
RNDP74 (2,547 m)	0.3°N,159.3°W	(22)	(22)	(22)[‡]	(22)	n/a	n/a

*Oxygen isotope records of cores ODP849 and TT013-PC72 are from benthic foraminifera; the oxygen isotope record of RNDP74 is measured on planktonic foraminifera.
[†]Age model of the upper 100 cm is based on ^{14}C AMS dating (10).
[‡]U/Th data were collected in samples older than 166 ky by α-spectrometry (22) but are not reported here because uncertainties become too large.
[§]Not available.